Korean Journal of Chemical Engineering (2024) 41:879–892
https://doi.org/10.1007/s11814-024-00081-w

ORIGINAL ARTICLE

Performance Evaluation of Static and Dynamic CO_2 Adsorption from Synthetic Gas Condensates Using Zinc Oxide, Silicon Dioxide and Zeolite 13X

Mohammad Reza Zaeri[1] · Feridun Esmaeilzadeh[1]

Received: 5 May 2023 / Revised: 1 August 2023 / Accepted: 3 September 2023 / Published online: 16 February 2024

Abstract
This paper evaluated ZnO, SiO_2 and zeolite 13X for removing CO_2 from normal heptane (nC_7) as synthetic gas condensates in batch mode. Based on the results of CO_2 adsorption isotherms, zeolite 13X had the highest CO_2 uptake in 1400–3700 ppm at atmospheric pressure. Due to the higher specific surface area of granular zeolite 13X, its CO_2 uptake was more than that of zeolite 13X powder. Also, the CO_2 adsorption equilibrium time was less than 30 min for zeolite 13X powder. The selectivity of zeolite 13X powder (i.e., H_2S/CO_2) was 2.36–4.08 for 2001–3930 ppm H_2S with 1668 ppm CO_2. Besides, the CO_2 breakthrough time for zeolite 13X powder was 50–4 min for WHSV (weight hourly space velocity) = 5–20 h^{-1} at 30 bar in continuous mode. Additionally, for the increased CO_2 concentration from 1000 to 3000 ppm, the CO_2 breakthrough time decreased from 30 to 11 min with WHSV = 10 h^{-1}. The CO_2 breakthrough time diminished by 2.5-fold as the pressure was reduced from 30 bar to atmosphere for the initial CO_2 concentration of 1000 ppm in nC_7 and WHSV = 10 h^{-1}. Subsequently, the regeneration of zeolite 13X by stagnant hot air was investigated for the CO_2 concentration range of 1000–3000 ppm, air-adsorbent contact time range of 30–180 min and temperature range of 100–300 °C using Box–Behnken design. Its regeneration efficiency was more than 95% for the CO_2 concentration below 1000 ppm.

Keywords Breakthrough · Carbon dioxide · Isotherm · Kinetics · Regeneration · Selectivity

Introduction

According to the gas condensates uses such as feedstock for olefin and BTX productions, plastic production and as a component to blend with fuels and due to large underground reserve of gas condensates, CO_2 as an inevitable impurity in gas condensate, which causes plugging pipelines by hydrate formation, product quality reduction and challenges in downstream catalytic processes such as reduction in the activity of catalysts and corrosion via bicarbonate ion formation by the reaction between water and CO_2 [1], should be removed. By the way, the standard recipes necessitate a reduction in CO_2 from petroleum products for exporting and other uses. Hence, there are several methods to remove CO_2 from gas condensates including adsorption [2, 3], membrane [4, 5], biologics [6, 7], fuel cell [8, 9], solvent treatment or absorption [10, 11] and hydrate formation [12, 13]. The heart of this paper is on the removal of CO_2 from synthetic gas condensates by adsorption for the sake of compatibility with feed pressure up to high, low content of CO_2 in terms of parts per million, prevalent and convenient conditions for regenerating adsorbent, adsorbent availability, no entrainment of adsorbent in gas condensates, ease of the separation of gas condensates from an adsorbent bed, slight pressure drop, no considerable change in feed temperature and no process challenges such as foaming and flooding. As far as we know, no experimental data for CO_2 removal from hydrocarbon liquids have been reported up to now. However, many attempts have been made for CO_2 removal from a gas mixture using different adsorbents including zeolite 13X, ZnO and SiO_2 by a variety of authors, but only those that were more or less successful are explained next. The

✉ Feridun Esmaeilzadeh
esmaeilzadeh95@gmail.com; esmaeil@shirazu.ac.ir

Mohammad Reza Zaeri
mr.zaeri2020@gmail.com

[1] Department of Chemical and Petroleum Engineering, School of Chemical, Petroleum and Gas Engineering, Enhanced Oil and Gas Recovery Institute, Advanced Research Group for Gas Condensate Recovery, Shiraz University, Shiraz 7134851154, Iran

results of CO_2 adsorption from normal heptane presented in this article can be utilized to investigate the CO_2 removal from hydrocarbon liquids such as gas condensates, NGLs, naphtha, etc.

Chue et al. conducted an experimental study on CO_2 adsorption from an N_2 gas mixture using two adsorbents of zeolite 13X and activated carbon. Zeolite 13X had a higher CO_2 uptake and favorable selectivity, so it is better for the bulk separation of CO_2 [14]. According to the study of CO_2 adsorption onto zeolite 13X and zeolite X/activated carbon (zeocarbon) using the static volumetric method under ambient condition, the CO_2 uptake on zeocarbon is just slightly higher than that of zeolite 13X [15]. Impregnating adsorbents such as zeolite 13X with amine chemicals augment their CO_2 adsorption capacity; however, weight loss of amine-impregnated adsorbents was very much compared to the unimpregnated ones (with a difference of approximately 20%) during temperature increased from ambient to below 200 °C. It poses a severe challenge to the regeneration of amine-impregnated zeolite 13X [16]. By evaluating the CO_2 adsorption from the N_2 gas mixture using the zeolites of 13X and 4A, zeolite 13X was better than 4A based on the CO_2 uptake. Because, the average pore size of zeolite 4A (i.e., 4 Å) is slightly larger than the kinetic diameter of the CO_2 molecule (i.e., 3.3 Å). Comparing the performance of zeolite 13X and activated carbon to adsorb CO_2 indicated that for low CO_2 partial pressure, the CO_2 uptake on zeolite 13X was higher than that of activated carbon. The CO_2/N_2 selectivity on zeolite 13X was higher than that of activated carbon. Besides, the CO_2 adsorption is reversible on zeolite 13X [17]. During the study accomplished by Bonenfant et al. (2008) on the CO_2 adsorption using various zeolite adsorbents including 13X, 5A, MCM-41, ZSM-5 and M-ZSM-5 (M = Li, Na, K, Rb and Cs), they understood that the zeolite 13X had the highest CO_2 adsorption capacity among the others [18]. Gholipour and Mofarahi (2016) investigated the CO_2 adsorption from a methane gas mixture on the surface of zeolite 13X. They discerned that by increasing pressure from 1 to 10 bar, the CO_2 uptake increased approximately 3.5 times more. They also demonstrated that at high pressure (i.e., 10 bar) as opposed to low pressure (i.e., 1 bar), the reduction of CO_2 adsorption capacity is less for zeolite 13X with the increased temperature [19].

By studying the CO_2 adsorption in different conditions of pressures (5–25 bar) and temperatures (25–100 °C) using ZnO, Kumar [20] recognized that the CO_2 uptake capacity of ZnO increased as the pressure was raised. However, the CO_2 adsorption on the ZnO surface increased with the incremental temperature. The highest CO_2 adsorption capacity was observed at 75 °C due to the augmentation of carbonation efficiency on the surface. The decomposition of carbonate species from the ZnO surface occurred at 250 °C when ZnO was regenerated. Finally, it was manifested that the ZnO adsorbent has favorable thermodynamics for CO_2 adsorption [20]. The CO_2 uptake onto ZnO adsorbent increased about 4.2 times more as the temperature was increased from 25 to 450 °C, which indicates that ZnO was suitable for CO_2 adsorption at high temperatures. According to the amount of CO_2 adsorption energy dissipated (i.e., -200 $kJ.mol^{-1}$), it was clear that CO_2 was chemically adsorbed on the surface of ZnO at high temperatures [21]. Tang and Luo investigated the molecular simulation of CO_2 adsorption on the surface of ZnO and confirmed that CO_2 adsorbed chemically via electron exchange [22].

Olivier and Jadot realized that the incremental CO_2 uptake on silica adsorbent was more significant than the adsorption capacity of other hydrocarbons such as methane, ethane and ethylene with increasing pressure [23]. The adsorption of CO_2 molecules often physically has occurred on the surface of silica due to dispersive and quadrupole interactions [24]. Silica has been coated with different amines for exalting the CO_2 adsorption capacity. However, this modification attenuated not only the thermal stability of the adsorbent as well as reduced its specific surface area [25]. Besides, modifying an adsorbent surface such as silica using amine sensitizes the CO_2 uptake to temperature so that the CO_2 adsorption capacity decreased as the temperature was raised above 60 °C [26]. Carvalho et al. found that silica, besides having a good adsorption capacity for CO_2, did not adsorb methane at all, so it was an excellent adsorbent for CO_2 removal from natural gas [27].

The previous research works reported in the literature are related to the CO_2 adsorption from the gas phase, while in this article, the CO_2 adsorption from the hydrocarbon liquid phase is evaluated. The CO_2 adsorption from a gas phase depends on the partial pressure of CO_2; however, the CO_2 adsorption from a liquid phase depends on the CO_2 concentration, or rather, CO_2 activity in the liquid [28]. As a result, the value of CO_2 adsorption capacity from a gas phase differs from that of a liquid phase. Therefore, it is essential to investigate the CO_2 adsorption from the hydrocarbon liquid phase of normal heptane as synthetic gas condensates. For this issue, the contributions of this article are summarized as follows:

- Investigation of the isotherms of CO_2 adsorption from the hydrocarbon liquid of $nC_7 + CO_2$ in the concentration range of 1400–3700 ppm by three adsorbents including zeolite 13X, silica and ZnO in order to choose a suitable adsorbent at room temperature and atmospheric pressure in batch mode.
- Appraisement of the kinetics of CO_2 adsorption from a mixture of $nC_7 + CO_2$ by the three aforementioned adsorbents at room temperature and atmospheric pressure in batch mode.
- The selectivity assessment of zeolite 13X to uptake CO_2 in the presence of H_2S at room temperature and atmospheric pressure in batch mode.

- Evaluation of the working efficiency of zeolite 13X, i.e., the characteristics of pressure effect and flow pattern including feed flow rate (WHSV = 5, 10, 15 and 20 h^{-1}), inlet CO_2 concentration (1000, 2000 and 3000 ppm) and particles size (i.e., powder and granule) of zeolite 13X on purification of the synthetic gas condensates from CO_2 in continuous mode.
- Regeneration of zeolite 13X by optimizing stagnant hot air temperature (100–300 °C) and air-adsorbent contact time (30–180 min) at different initial concentrations of CO_2 (1000–3000 ppm) with the help of Box–Behnken design under atmospheric pressure.

Experimental

Materials

The following chemicals were bought from Sigma-Aldrich: iron sulfide (FeS, purity > 99%), calcium carbonate ($CaCO_3$, purity > 99%), hydrochloric acid (HCl, with a purity of 37%, the density of 1.19 g mL^{-1}), normal heptane (n-heptane, nC_7, purity > 99%, the density of 0.67 g mL^{-1}), sodium hydroxide (NaOH, purity > 99%) and phenolphthalein (0.001 g ml^{-1} in ethanol/water of 50:50%) as an indicator. Zinc oxide (ZnO) was purchased from the Scharlau Company, Spain, with a purity of more than 99.99%. Silica (SiO_2) was used as received from Nanosany Corporation, Iran, with an apparent particle size of 20–30 nm, purity of > 99%, a specific surface area of 180 ~ 600 m^2 g^{-1}, bulk density < 0.1 g.cm^{-3} and a true density of 2.4 g cm^{-3}. Zeolite 13X (grinded to make powder with a particle size of 50–290 microns, granule with a diameter of 1.6–2.5 mm) was used as donated by Gaharceram Company, Iran. All materials were used as received without further purification.

Characterization of Adsorbent

Adsorption/desorption of N_2 gas at 77 Kelvin in the BET analysis evaluated the specific surface area, pore size and pore volume for all adsorbents. About 0.1 g of each adsorbent was first dehumidified at 120 °C for 2 h and consecutively degassed in situ under vacuum. Next, the BET analysis was performed with the Belsorp mini II apparatus made by MicrotracBel Corporation, Japan.

The thermal stability of the zeolite 13X was appraised by thermogravimetric analysis (TGA) and differential scanning calorimetric analysis (DSC) based on the weight loss of the adsorbent via applying heat. After placing about 4 mg of the adsorbent in a platinum crucible linked to a sensitive balance installed in a furnace, the heat was exerted with a constant rate of 10 °C.min^{-1} at argon gas medium to achieve up to 600 °C utilizing the TGA-Q600 apparatus made by TA Instruments Company, USA. The maximum temperature before starting the degradation of the adsorbent was determined by TGA analysis. The DSC analysis was conducted to identify whether to absorb or produce heat during the adsorbent weight change.

Adsorption Performance in CO_2 Removal from nC_7

Batch Mode

The synthetic sour gas condensates were prepared by blowing CO_2 or H_2S into 150 mL of nC_7 existed in a 250-mL graduated cylinder for 15 and 40 min, respectively, for CO_2/nC_7 and H_2S/nC_7 at ambient condition. An amount of 13 g of FeS powder (with a grinding degree of 50–300 mesh) was reacted with 20 mL of HCl to produce H_2S gas. CO_2 was prepared by a reaction between 9.5 g of $CaCO_3$ and 20 mL of HCl. The concentrations of H_2S and CO_2 were 7500 and 3300 ppm, respectively.

To study the isotherm and kinetics of each adsorbent including zeolite 13X, SiO_2 and ZnO, for CO_2 adsorption at ambient condition in batch mode, 26.5 mL of synthetic sour gas condensates with the specified CO_2 concentration (i.e., 1400–3700 ppm) was contacted to 0.05 g of the adsorbent in a 25-mL glass balloon. The total volume of the glass balloon is 27.5 mL up to its cap. In order not to create void volume, the glass balloon was filled up to its cap, taking into account the volumes of the magnet and adsorbent. An amount of early sour nC_7 including 26.5, 22, 17 and 12.5 mL was added to pure nC_7 to achieve a constant volume of 26.5 mL for preparing sour gas condensates containing CO_2 with the concentration of ~ 3700, 3071, 2373 and 1745 ppm, respectively. Next, the system was stirred on a magnetic stirrer at 400 rpm. A time of 24 h was allocated for the investigation of the adsorption isotherm, and the incremental times (i.e., 3, 5, 10, 20, 30, 60 and 90 min) were assigned to evaluate the adsorption kinetics. CO_2 concentration in nC_7 was measured before and after contacting the adsorbent to the sour gas condensates to determine the CO_2 uptake. Four equilibrium points are obtained at each time of studying the isotherm. The isotherm assessment was carried out twice for each of the adsorbents. The concentration of CO_2 and H_2S in nC_7 was measured according to the ASTM standard methods of D664 based on acid–base titration and D3227 based on Volhard's argentometric back titration, respectively. Formulas (1) and (2) represent the CO_2 adsorption capacity in terms of $mgCO_2$ per gram of the adsorbent and $mgCO_2$ per square

meter of the specific surface area of the adsorbent, respectively. Formula (3) indicates the selectivity of an adsorbent for CO_2 adsorption in the presence of H_2S.

$$q_e = \frac{\rho_s \times V_s}{1000 \times M_{ads}} \left(X_0 - X_f\right) \tag{1}$$

$$Q_e = q_e / S_a \tag{2}$$

$$\text{Selectivity} = q_{e,H_2S}/q_{e,CO_2} \times \left(\frac{M_{w,CO_2}}{M_{w,H_2S}}\right) \tag{3}$$

where X_0 is the initial concentration of CO_2 (ppm CO_2), X_f is the equilibrium (final) concentration of CO_2 (ppm CO_2), ρ_s is the density of nC_7 (g mL^{-1}), V_s is the volume of the organic phase (mL), M_{ads} is the weight of the adsorbent (g) and S_a is the specific surface area of the adsorbent (m^2 g^{-1}). q_{e,H_2S} and q_{e,CO_2} are the adsorption capacities for H_2S and CO_2 in terms of mg g^{-1}, respectively. M_w represents the molecular weight (g mol^{-1}).

Continuous Mode

To investigate the CO_2 breakthrough, 2 g of zeolite 13X was loaded in a stainless steel cylindrical column with a diameter of 1 cm and a volume of 11.781 cm^3. Then, by a high-pressure syringe pump (model: Agilent HPLC pump, series 1200, USA), the sour gas condensates containing CO_2 with a certain concentration were passed through the adsorbent bed (see Fig. 1). In order to detect the presence of CO_2 and its concentration at the exit of the adsorption column (i.e., 200, 400, 600, 800 and 1000 ppm CO_2 in 1.5 mL of nC_7 neutralized for investigating the WHSV effect), the NaOH solution with a certain concentration along with an indicator of phenolphthalein was used due to the reaction between CO_2 molecules and OH^- ions in a gas washing bottle. The experiment was continued until the color of the aqueous solution shifted from purple to colorless. The flow patterns, including the liquid flow rate of the synthetic sour gas condensates (WHSV = 5, 10, 15 and 20 h^{-1} corresponding to 0.167, 0.334, 0.502 and 0.670 mL min^{-1}, respectively), the inlet CO_2 concentration (1000, 2000 and 3000 ppm) and particle size of zeolite 13X (powder and granule of zeolite 13X), were evaluated with the help of analyzing the

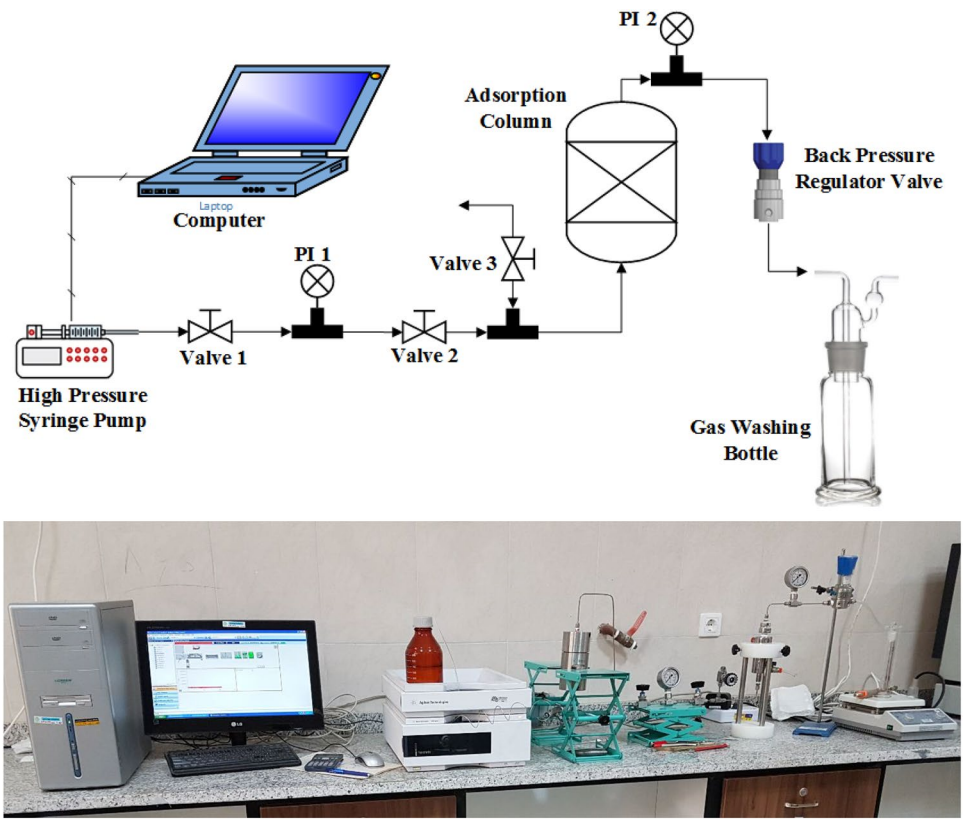

Fig. 1 Continuous adsorption setup for the atmosphere and high pressure

CO_2 breakthrough curves. Also, the effect of pressure (i.e., atmospheric pressure and 30 bar) on the CO_2 breakthrough was investigated. The dynamic and breakthrough capacities were estimated by Formulas (4) and (5), respectively. Formula (6) was employed to calculate the length of the unused bed per total length of the bed [29].

$$\begin{aligned} \mathrm{Cap}_{dyn} &= \frac{\mathrm{WHSV} \times C_{\mathrm{in}}}{6 \times 10^4} \times \int_0^{\infty} \left(1 - C_{\mathrm{exit}}/C_{\mathrm{in}}\right) dt \\ &\simeq \frac{\mathrm{WHSV} \times C_{\mathrm{in}}}{12 \times 10^4} \times \left(t_{br} + t_e\right) \end{aligned} \tag{4}$$

$$Cap_{br} = \mathrm{WHSV} \times C_{\mathrm{in}} \times \int_0^{t_{br}} \left(1 - C_{\mathrm{exit}}/C_{\mathrm{in}}\right) dt \simeq \frac{\mathrm{WHSV} \times C_{\mathrm{in}} \times t_{br}}{6 \times 10^4} \tag{5}$$

$$\frac{LUB}{Z} = 1 - \eta = 1 - \frac{\mathrm{Cap}_{br}}{Cap_{dyn}} \simeq \frac{t_e - t_{br}}{t_{br} + t_e} \tag{6}$$

where the WHSV is the weight hourly space velocity of the fluid (h^{-1}), C_{in} is the inlet concentration of CO_2 (ppm), C_{exit} is the outlet concentration of CO_2 (ppm), t is time (min), t_{br} is the starting point of the curvature in the breakthrough (min), t_{e} is the endpoint of the curvature in the breakthrough (min) and η is the adsorption efficiency of an adsorbent bed.

Regeneration of Adsorbent

The stagnant hot air contact method was performed for the thermal regeneration of zeolite 13X by optimizing the governing variables including hot air temperature (100–300 °C) and contact time (30–180 min) for an initial CO_2 concentration (1000–3000 ppm) with the Box–Behnken design at atmospheric pressure. The hot air was supplied using a smart oven that can record temperature, and it is programmable in the range of 35–350 °C with a precision of 1 °C (model: ATRA, Iran). The criterion for determining optimal values of variables was the ratio of the CO_2 uptake on the regenerated adsorbent per CO_2 uptake on the fresh adsorbent at atmospheric pressure in batch mode.

Table 1 Results of BET analysis for SiO_2, ZnO and zeolite 13X adsorbents

Sample	S_{BET} ($m^2\ g^{-1}$)	V_{pore} ($cm^3\ g^{-1}$)	$d_{\mathrm{pore,ave}}$ (nm)
SiO_2	294	1.179	16.042
ZnO	5	0.017	14.308
Zeolite 13X powder	111	0.151	5.470
Granular zeolite 13X	527	0.287	2.176

Results and Discussion

Adsorbent Characterization

According to the IUPAC classification of materials, the SiO_2 adsorbent with a specific surface area of 294 $m^2\ g^{-1}$, a pore volume of 1.18 $cm^3\ g^{-1}$ and a pore diameter of 16.04 nm (see Table 1) are in the category (II) pursuant to what was apprehended in Fig. 2 based on the shape of N_2 adsorption/desorption curve. Therefore, SiO_2 has mesopores and unlimited mono-multilayer adsorption. The ZnO adsorbent with a minimum specific surface area of 5 $m^2\ g^{-1}$, a minimum pore volume of 0.02 $cm^3.g^{-1}$ and a pore size of 14.31 nm is in the category (III); hence, ZnO has mesopores. In addition, zeolite 13X powder with a specific surface area of 111 $m^2\ g^{-1}$, a pore volume of 0.15 $cm^3\ g^{-1}$ and a pore size of 5.47 nm are in the category (II), indicating that it has mesopores and traps [29].

Based on the position of inflection points in Fig. 2, it is evident that the silica adsorbent is a pioneer in the N_2 monolayer adsorption. However, this feature is improved for the granular zeolite 13X. The lack of hysteresis in the N_2 adsorption/desorption for ZnO indicates the absence of low-size pores, no long cavities and no large pore volume, which has provided the possibility of the complete N_2 recovery. Of course, the high pore volume of granular zeolite 13X provides the covering of hysteresis compared to zeolite 13X powder. The cage-like structure of zeolite 13X prevents easily escaping of trapped molecules, thereby appearing as a negligible hysteresis. However, increasing temperature raises the kinematic energy of the trapped molecules, allowing more molecules to be recovered. The granulation of an adsorbent has made two dominant factors better in the adsorption: specific surface area and pore volume. Because, the specific surface area is very effective on the monolayer uptake; also, the large pore volume and the appropriate pore diameter provide multilayer adsorption; furthermore, the pore diameter controls the evasion of adsorbed molecules.

CO_2 Adsorption Isotherm

Figure 3 depicts the CO_2 adsorption from synthetic gas condensates by various adsorbents including SiO_2, ZnO, zeolite 13X powder and granular zeolite 13X at room temperature and atmospheric pressure. Zeolite 13X has the highest CO_2 adsorption capacities at an initial CO_2 concentration range of 1400–3700 ppm. According to Table 2, all adsorbents follow the Freundlich isotherm with a determined coefficient of more than 0.96, except ZnO, which obeyed the Temkin isotherm with a determined coefficient of more than 0.95. The small specific surface area of ZnO and its CO_2 adsorption capacity based on the specific surface area compared to the

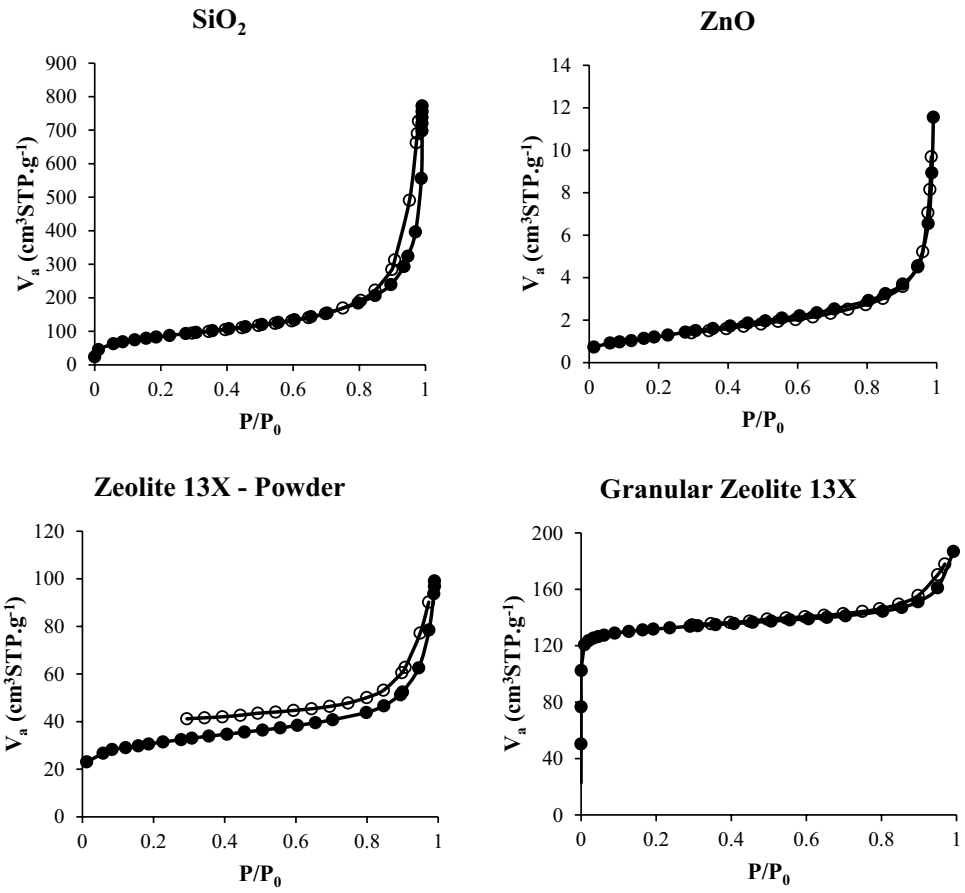

Fig. 2 N_2 adsorption/desorption graphs for SiO_2, ZnO and zeolite 13X adsorbents; (solid circle) adsorption and (hollow circle) desorption

other adsorbents indicates the physical multilayer adsorption of CO_2 on the ZnO surface. Because the monolayer adsorption capacity of CO_2 is very restricted due to the unavailability of sufficient specific surface area, this issue indicates the attraction between zinc element and CO_2. Thus, its adsorption force range is the highest compared to SiO_2 and zeolite 13X. The heat released during the CO_2 adsorption on ZnO based on Temkin's parameter of *b* demonstrates the physical adsorption because large amounts of energy (approximately more than 40 kJ mol^{-1}) are released during the chemical adsorption. However, zeolite 13X had a significant CO_2 uptake due to its more specific surface area and tetrahedral pore structure, thereby enabling to adsorb CO_2 as mono-multilayer adsorption and trapping CO_2. Granular zeolite 13X had more CO_2 monolayer adsorption capacity than powdered one owing to its larger specific surface area. However, due to its smaller pore size compared to zeolite 13X powder, the number of CO_2 layers is less. CO_2 molecules are often captured inside the structure of granular zeolite 13X. In fact, the appropriate pore diameter for granular zeolite 13X causes CO_2 molecules to trap and not to exit. Also, the large pore volume of granular zeolite 13X has provided favorable condition for CO_2 storage. Comparing the heat dissipated during CO_2 adsorption between the two types of zeolite confirms the provision of better condition for CO_2 capture by granular zeolite 13X. Eventually, the zeolite 13X adsorbent was chosen as an excellent candidate for CO_2 adsorption from gas condensates.

CO_2 Adsorption Kinetics and Selectivity of Zeolite 13X

The kinetics of CO_2 adsorption were investigated under room temperature and atmospheric pressure using different adsorbents including silica, ZnO and zeolite 13X, to apperceive the equilibrium time. Results of the kinetics are shown in Fig. 4. The equilibrium time for all types of adsorbents is less than 30 min indicating the desired adsorption rate. Therefore, zeolite 13X has a proper tendency to adsorb CO_2. The equilibrium time decreases for zeolite 13X by declining the initial CO_2 concentration. Additionally, as the CO_2 adsorption capacity reduces, a shorter time is needed to reach the saturation point of CO_2 uptake.

The presence of CO_2 along with H_2S in the gas condensates is unavoidable, so studying the competitive adsorption of these compounds on the surface of zeolite 13X is

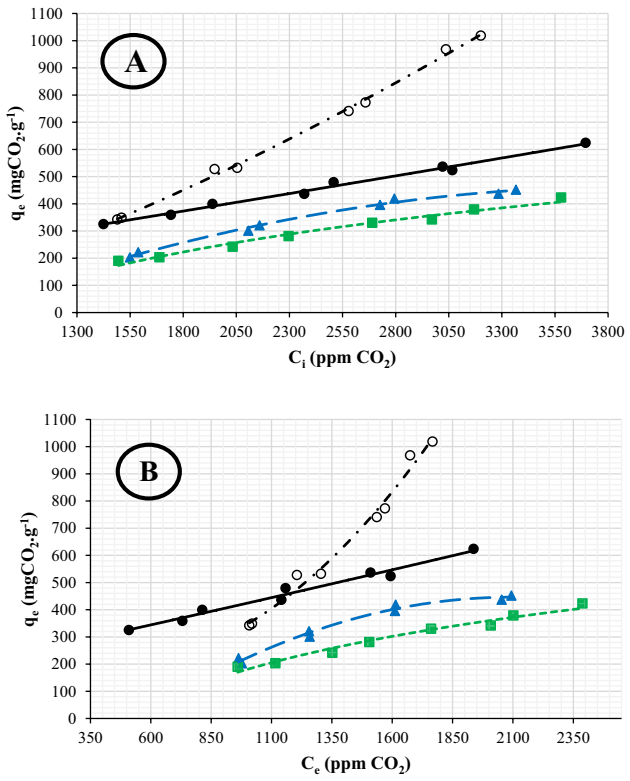

Fig. 3 CO_2 adsorption recorded at room temperature and atmospheric pressure on SiO_2 (square), ZnO (triangle), zeolite 13X powder (solid circle) and granular zeolite 13X (hollow circle); based on (A) the initial CO_2 concentration and (B) the equilibrium CO_2 concentration

essential. Therefore, the selectivity of zeolite 13X powder was evaluated for CO_2 adsorption in the presence of H_2S under room temperature and atmospheric pressure. To this end, the CO_2 concentration was kept constant (1668 ppm CO_2), and different H_2S concentrations were considered 3930, 2807 and 2001 ppm. Figure 5 shows the results of the selectivity study of zeolite 13X powder. The selectivity of zeolite 13X with values greater than 2.36 indicates the high tendency of the adsorbent surface to uptake H_2S against CO_2. Actually, zeolite 13X powder has a mineral surface, so it tends to adsorb polar compounds such as H_2S. On the other hand, a non-polar compound like CO_2 has more tendency to be present in an organic phase of nC_7.

Breakthrough Evaluation in CO_2 Removal from Synthetic Gas Condensates Using Zeolite 13X

The CO_2 adsorption efficiency of the adsorbent bed of zeolite 13X was appraised at room temperature and 30 bar with 1000 ppm CO_2 concentration by analyzing its breakthrough curves. As shown in Fig. 6, the results exhibit a decline in the CO_2 breakthrough time from 50 to 4 min as well as the mass transfer zone with the increased WHSV from 5 to 20 h^{-1}. This is due to insufficient contact time between CO_2 molecules and zeolite 13X surfaces. The adsorption is a slow phenomenon and based on the adsorption kinetics, at least

Table 2 The parameters were evaluated from the interpolation of CO_2 adsorption isotherms

Isotherm	Parameter	SiO_2	ZnO	Zeolite 13X powder	Granular zeolite 13X
Freundlich	K_F (mgCO_2 g^{-1} ppm^{-n})	0.363	0.261	15.775	5.975×10^{-4}
	n	0.907	0.984	0.480	1.918
	R^2	***0.9871***	0.9242	***0.9677***	***0.9856***
Langmuir	q_m (mgCO_2 g^{-1})	2611	−4929	799	−616
	K_L (ppm^{-1})	7.878×10^{-5}	-4.419×10^{-5}	1.254×10^{-3}	-3.593×10^{-4}
	R^2	0.9841	0.9329	0.9389	0.9833
Temkin	K_T (ppm^{-1})	2.014×10^{-3}	2.107×10^{-3}	7.841×10^{-3}	1.298×10^{-3}
	B (J mol^{-1} mg^{-1}CO_2 g)	9.599	7.899	11.501	2.137
	R^2	0.9707	***0.9561***	0.9399	0.9537
Temkin's heat adsorption (kJ.mol^{-1})		1.82–4.06	1.60–3.57	3.74 ~ 7.18	0.73–2.18
Monolayer capacity (mgCO_2 g^{-1})		251.21	4.17	94.60	450.56
No. of layers of CO_2 on the adsorbent surface		1–2	48–109	3–7	1–3
Adsorption force range *(nanometer)*		0.33–0.66	15.84–35.97	0.99–2.31	0.33–0.99
Capacity (mgCO_2 cm^{-2}) wrt. (C_i = 1400–3700 ppm CO_2)		0.65–1.44	41.60–92.62	2.93–5.63	0.65–1.93
$\ln q_e = \ln K_F + n \times \ln C_e$		$\frac{1}{q_e} = \frac{1}{q_m} + \frac{1}{q_m \times K_L} \times \frac{1}{C_e}$			
$q_e = \frac{RT}{b}\ln K_T + \frac{RT}{b} \times \ln C_e$		$q_{\text{monolayer}}(mgCO_2/g) = \frac{176\times10^{23}\times S_{BET}}{\pi\times d_{CO_2}^2\times N_A} = 0.8542 \times S_{BET}(m^2/g)$			

No. of layers of CO_2 on the adsorbent surface $= q_e / q_{monolayer}$

Adsorption force range = (No. of layers of CO_2) × (Molecular diameter of CO_2)

*The molecular diameter of CO_2 is 3.3 angstroms [30]

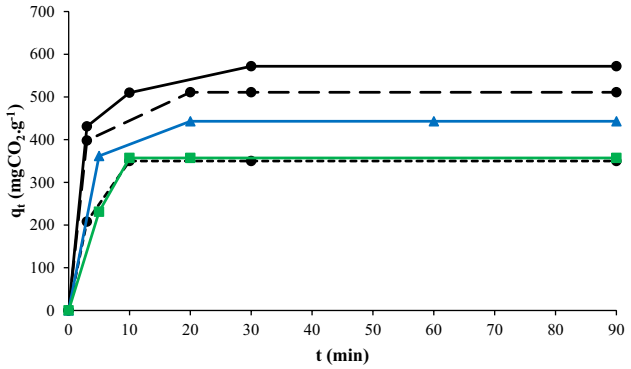

Fig. 4 CO_2 adsorption kinetics at room temperature and atmospheric pressure for SiO_2 (green square, 3029-ppm CO_2); ZnO (blue triangle, 3308-ppm CO_2) and zeolite 13X powder: 3333-ppm CO_2 (black circle, solid line), 2862-ppm CO_2 (black circle, dashed line) and 1621-ppm CO_2 (black circle, dotted line)

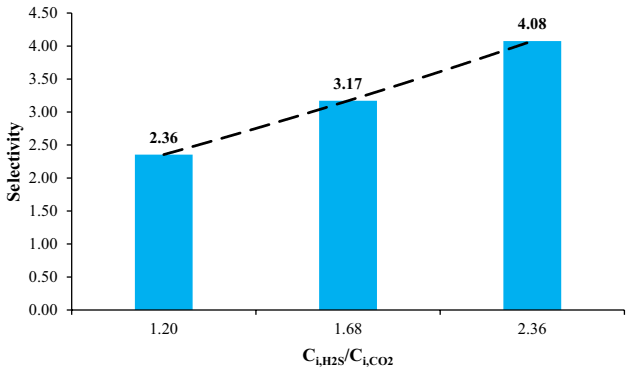

Fig. 5 Selectivity assessment of zeolite 13X powder for CO_2 removal from the synthetic gas condensates in the presence of H_2S at ambient condition

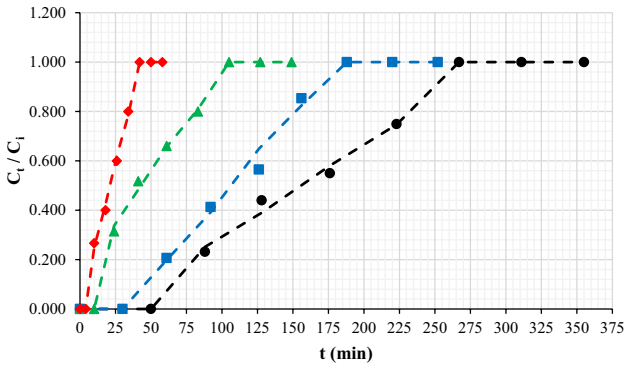

Fig. 6 CO_2 breakthrough curves for zeolite 13X powder at room temperature and 30 bar with the inlet CO_2 concentration of 1000 ppm and the different WHSVs including 5 h^{-1} (black circle, t_{br} = 50 min), 10 h^{-1} (blue square, t_{br} = 30 min), 15 h^{-1} (green triangle, t_{br} = 10 min) and 20 h^{-1} (red rhombus, t_{br} = 4 min); (points) experimental data, (dashed line) curve fitted data using the Thomas model

30 min is needed to establish the equilibrium between the adsorbent and the adsorbate. The Thomas model was well fitted to the experimental data with a determined coefficient of more than 0.96, and the details are provided in Table 3. The k_{th} parameter increases by raising the WHSV. In fact, the k_{th} parameter has a direct relationship with the overall mass transfer coefficient. Thus, as the mass transfer rate increases, the length of the mass transfer zone decreases. As mentioned above, sufficient time is impossible to achieve the solid/liquid phase equilibrium by increasing the WHSV. Hence, the distance between the working and equilibrium points increases, and as a result, the CO_2 uptake decreases roughly. By increasing the WHSV, the CO_2 breakthrough time decreases (a negative impact) as well as the length of the mass transfer zone (a positive impact). Therefore, the length of the unused bed (LUB/Z) first increases with the increased WHSV and then remains constant.

Figure 7 shows the results of the inlet CO_2 concentration effect (1000, 2000 and 3000 ppm) on CO_2 breakthrough time for zeolite 13X powder at 30 bar and room temperature with WHSV of 10 h^{-1}. Actually, the increased inlet CO_2 concentration has caused a reduction in the CO_2 breakthrough time and a diminution in the mass transfer zone. However, the results indicate that the change in the mass transfer zone is roughly lost under the increment of inlet CO_2 concentration with a value of more than 2000 ppm. According to the results of the kinetics adsorption, with the increase in initial CO_2 concentration, more time is required to establish the phase equilibrium of liquid/solid. Therefore, the distance between the working and equilibrium points increases, thereby reducing the CO_2 breakthrough time. The symmetric shape of the mass transfer zone in the CO_2 breakthrough curves indicates that the CO_2 overall mass transfer coefficient is constant during CO_2 adsorption from the organic phase onto the solid phase.

The effect of pressure on CO_2 adsorption for zeolite 13X is shown in Fig. 8 at a concentration of 1000-ppm CO_2 in continuous mode. As can be seen, when the pressure of adsorption reduced from 30 to 1 bar, the CO_2 breakthrough time decreased by 2.5-fold for zeolite 13X powder, which caused the reduction in the mass transfer zone. By comparing the data in Table 4, the changes in the adsorption capacity between two pressures of 30 and 1 bar indicate the dominance of multilayer physical adsorption for CO_2 uptake on the zeolite 13X. The comparison of CO_2 adsorption between granular and powder zeolite 13X is presented in Fig. 8. It shows the channeling incidence in the adsorbent bed of the granular zeolite 13X. This event reduced the CO_2 breakthrough time and increased the length of the mass transfer zone. The CO_2 breakthrough time reduction for granular zeolite 13X was more than its powder under

Table 3 Parameters of the Thomas model for the inlet CO_2 concentration of 1000 ppm at various WHSVs (5–20 h^{-1})

WHSV (h^{-1})	k_{th} (ppm^{-1} min^{-1})	q_{max} ($mgCO_2.g^{-1}$)	R^2	Cap_{br} ($mgCO_2$ g^{-1})	Cap_{dyn} ($mgCO_2$ g^{-1})	$LUB/Z(\%)$
5	1.610×10^{-5}	12.97	0.9744	4.16	13.20	68.45
10	3.100×10^{-5}	17.68	0.9640	5.00	18.15	72.48
15	3.580×10^{-5}	10.73	0.9871	2.50	14.39	82.61
20	1.001×10^{-4}	7.03	0.9891	1.34	7.68	82.61

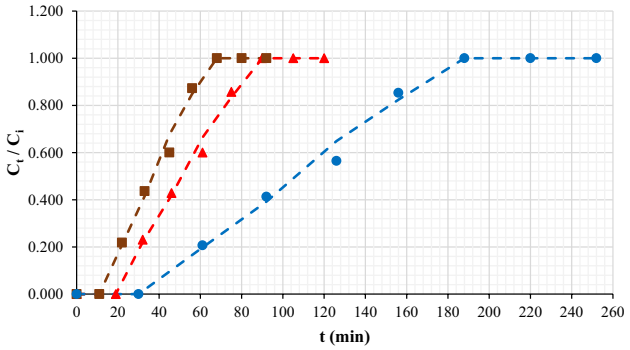

Fig. 7 CO_2 breakthrough curves for zeolite 13X powder at room temperature and 30 bar with the WHSV = 10 h^{-1} for the various inlet CO_2 concentrations including 1000 ppm (blue circle, t_{br} = 30 min), 2000 ppm (red triangle, t_{br} = 19 min) and 3000 ppm (brown square, t_{br} = 11 min); (points) experimental data, (dashed line) curve fitted data using the Thomas model

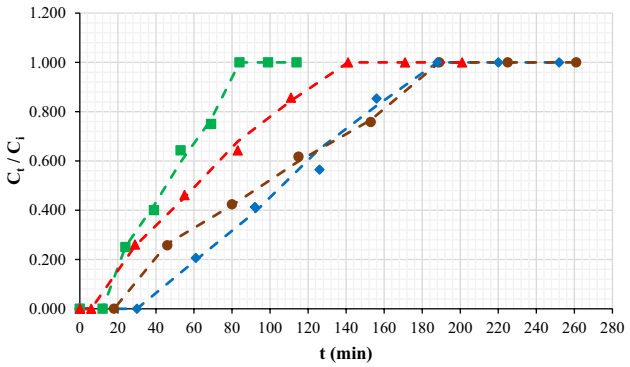

Fig. 8 CO_2 breakthrough curves for zeolite 13X of powder and granule at room temperature and two different pressures, i.e., 30 bar and the atmospheric pressure, with the WHSV = 10 h^{-1} and the inlet CO_2 concentration of 1000 ppm; powder and 30 bar (blue rhombus, t_{br} = 30 min), granule and 30 bar (brown circle, t_{br} = 18 min), powder and atmosphere (green square, t_{br} = 12 min) and granule and atmosphere (red triangle, t_{br} = 6 min); (points) experimental data, (dashed line) curve fitted data using the Thomas model

pressure changed from 30 to 1 bar. The decline of the CO_2 breakthrough time between the powder and granular zeolite 13X is lower at 30 bar compared to its value at 1 bar, indicating the influence of pressure to compensate for this reduction.

Regeneration of Zeolite 13X

The stagnant hot air contact method was executed for regenerating zeolite 13X powder contaminated with CO_2 under atmospheric pressure. TGA and DSC were used to analyze the thermal degradation behavior of zeolite 13X in order to obtain the maximum air temperature, which can be used for its regeneration. According to the TGA and DSC profiles shown in Fig. 9, zeolite 13X has no thermal degradation up to a temperature of 500 °C. Therefore, the hot air temperature in the range of 100–300 °C was considered for the regeneration of zeolite 13X powder.

In order to determine optimal conditions for the regeneration of zeolite 13X powder contaminated with CO_2 at the initial concentration range of 1000–3000 ppm, the hot air temperature and contact time were kept in the range of 100–300 °C and 30–180 min, respectively. Table 5 shows the values of variables governing the regeneration of zeolite 13X powder including hot air temperature, contact time and initial CO_2 concentration, by applying the Box–Behnken design. Afterward, 15 experiments were designed. The response values (i.e., the ratio of the CO_2 uptake of the regenerated adsorbent to the CO_2 uptake of the fresh adsorbent) for each experiment are shown in Table 6.

After applying the ANOVA to the experimental data provided in Table 7, a reduced quadratic model was obtained to define the relationship between the variables governing the regeneration of zeolite 13X powder. The p-value of the presented regeneration model is less than 0.05, which indicates that the regeneration model is significant. The p-value of the residuals is greater than 0.05, confirming no difference between the predicted values and the experimental data. The determined coefficients of the model with a value of more than 0.947 are close enough to the value of one. Therefore, Formula (7) can be used to determine optimal regeneration conditions of zeolite 13X for different amounts of initial CO_2 concentration up to 3000 ppm.

Figure 10 shows the diagnosis plots including the residuals vs. predicted plot, normal plot of residuals and predicted vs. actual plot. The residuals between the experimental data and the predicted values from the regeneration model have a normal distribution indicating no data scatter. The regeneration model can predict the response values because, in the

Table 4 Parameters of the Thomas model for different inlet CO_2 concentrations (1000 ~ 3000 ppm) at two different pressures (i.e., atmospheric pressure and 30 bar) with the WHSV of 10 h^{-1}

Type of zeolite 13X	C_{CO_2}(ppm CO_2)	P (bar)	k_{th} (ppm^{-1} min^{-1})	q_{max} ($mgCO_2$ g^{-1})	R^2	Cap_{br} ($mgCO_2$ g^{-1})	Cap_{dyn} ($mgCO_2$ g^{-1})	LUB/Z(%)
Powder	1000	30	3.100×10^{-5}	17.68	0.9640	5.00	18.15	72.48
Powder	2000	30	3.355×10^{-5}	16.95	0.9769	6.33	18.15	65.14
Powder	3000	30	2.993×10^{-5}	18.38	0.9704	5.49	19.73	72.15
Granule	1000	30	2.070×10^{-5}	15.93	0.9966	3.00	17.23	82.61
Granule	1000	1	3.370×10^{-5}	10.12	0.9911	1.00	12.24	91.84
Powder	1000	1	5.070×10^{-5}	7.55	0.9803	2.00	8.00	75.00

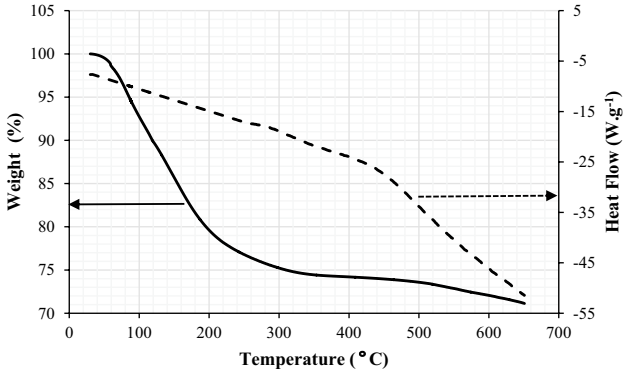

Fig. 9 TGA and DSC analyses for zeolite 13X powder in argon

predicted vs. actual plot, the data are matched on a straight line with an angle of 45°, and the average relative error of the regeneration model is less than 3%, according to the residuals vs. predicted plot.

The optimal values of the hot air temperature and contact time were determined for three initial CO_2 concentrations including 1000, 2000 and 3000 ppm, to ensure the predictive validity of the regeneration model based on Formula (7). The samples of zeolite 13X powder contaminated with CO_2 were then regenerated under the same conditions. Results are shown in Table 8. Results indicate the excellent predictability of the model for the regeneration of zeolite 13X powder.

According to the perturbation plot shown in Fig. 11, the regeneration efficiency of zeolite 13X is strongly influenced by the initial CO_2 concentration. So that by increasing the initial CO_2 concentration, the regeneration efficiency of the adsorbent decreased. However, increasing hot air temperature or contact time improves the adsorbent regeneration efficiency. Of course, the increased temperature can compensate for the regeneration efficiency reduction more than raising the contact time. For the initial concentration of 1000-ppm CO_2, the regeneration efficiency of zeolite 13X is more than 95%. However, for the initial CO_2 concentration of 2000 ppm, the hot air temperature must be more than 225 °C for 60 min to achieve more than 95% regeneration efficiency.

Conclusions

In this research, the CO_2 adsorption from nC_7 as a candidate of gas condensates was investigated at room temperature and atmospheric pressure by ZnO, SiO_2 and zeolite 13X adsorbents in batch mode. Results indicated the superiority of zeolite 13X due to the highest CO_2 adsorption capacity. The CO_2 adsorption equilibrium time was 10, 20 and 30 min, corresponding to the initial CO_2 concentration of 1621, 2862 and 3333 ppm, respectively, using zeolite 13X powder. Although zeolite 13X was the superior adsorbent for removing CO_2 from the synthetic gas condensate, zeolite 13X showed a great tendency to uptake H_2S in the competitive adsorption of CO_2/H_2S. So, the zeolite 13X selectivity value was more than 2.36 up to 4.08. The surface of zeolite 13X is mineral, so it shows a great tendency to adsorb a polar molecule like H_2S compared to a non-polar molecule such as CO_2.

As the WHSV of the synthetic gas condensates increased, the CO_2 breakthrough time for zeolite 13X powder decreased at room temperature and 30 bar, and the mass transfer zone became small. The CO_2 breakthrough time decreased from

Table 5 The range of the coded variables affects the regeneration of zeolite 13X powder using the stagnant hot air contact method by applying the Box–Behnken design

Variable	Range (unit)	The variable level		
		−1	0	+1
Initial concentration of CO_2 (A)	1000–3000 (ppm CO_2)	1000	2000	3000
Hot air temperature (B)	100–300 (°C)	100	200	300
Contact time (C)	30–180 (min.)	30	105	180

Table 6 Box–Behnken design matrix and experimental results for regenerating zeolite 13X powder contaminated with CO_2 using the stagnant hot air contact method

STD	Initial concentration of CO_2 (*A*) (ppm CO_2)	Hot air temperature (*B*) (°C)	Contact time (*C*) (min.)	Capacity of the regenerated zeolite 13X powder ($mgCO_2\ g^{-1}$)	Response (%)
1	1000	200	30	262.83	96.92
2	1000	200	180	267.00	98.46
3	1000	100	105	258.65	95.38
4	1000	300	105	268.39	98.97
5	2000	100	30	358.02	90.00
6	2000	100	180	369.95	93.00
7	2000	300	30	370.95	93.25
8	2000	300	180	382.88	96.25
9	2000	200	105	376.92	94.75
10	2000	200	105	375.92	94.50
11	2000	200	105	377.91	95.00
12	3000	200	30	472.37	89.06
13	3000	200	180	483.35	91.13
14	3000	100	105	469.35	88.49
15	3000	300	105	498.36	93.96

q_e (C_i = 1000 ppm CO_2) = 271.18 $mgCO_2\ g^{-1}$
q_e (C_i = 2000 ppm CO_2) = 397.80 $mgCO_2\ g^{-1}$
q_e (C_i = 3000 ppm CO_2) = 530.40 $mgCO_2\ g^{-1}$

Table 7 ANOVA for reduced quadratic model and transform of response, power-law with the lambda equal to 3, for regenerating zeolite 13X powder contaminated with CO_2 using the stagnant hot air contact method

Source	Sum of squares	*df*	Mean square	p-value	Expl.
Model	9.491×10^{10}	4	2.373×10^{10}	< 0.0001	Significant
A	6.415×10^{10}	1	6.415×10^{10}	< 0.0001	
B	2.076×10^{10}	1	2.076×10^{10}	< 0.0001	
C	7.854×10^{9}	1	7.854×10^{9}	0.0010	
C^2	2.149×10^{9}	1	2.149×10^{9}	0.0365	
Residual	3.694×10^{9}	10	3.694×10^{8}		
Lack of fit	3.603×10^{9}	8	4.504×10^{8}	0.0946	Not significant
Pure error	9.067×10^{7}	2	4.534×10^{7}		
Correlation total	9.861×10^{10}	14			
Fit statistics					
Std. Dev	19,219.63	Mean	8.317×10^{5}	C.V. %	2.31
R^2	0.9625	Adjusted R^2	0.9476	Adeq. precision	25.7167
Coded Formula (7)					

$$(\text{Regenerability})^3 = 8.445\times10^5 - 89550.27\times A + 50935.95\times B + 31332.8\times C - 23994.91\times C^2$$

Actual Formula (7)

$$(\text{Regenerability})^3 = 8.3083\times10^5 - 89.5503\times C_{CO_2} + 509.3595\times T_{air} + 1313.5808\times t - 4.2658\times t^2$$

*p-value ≤ 0.001 highly significant; 0.001 < p-value ≤ 0.05 significant and p-value > 0.05 not significant.

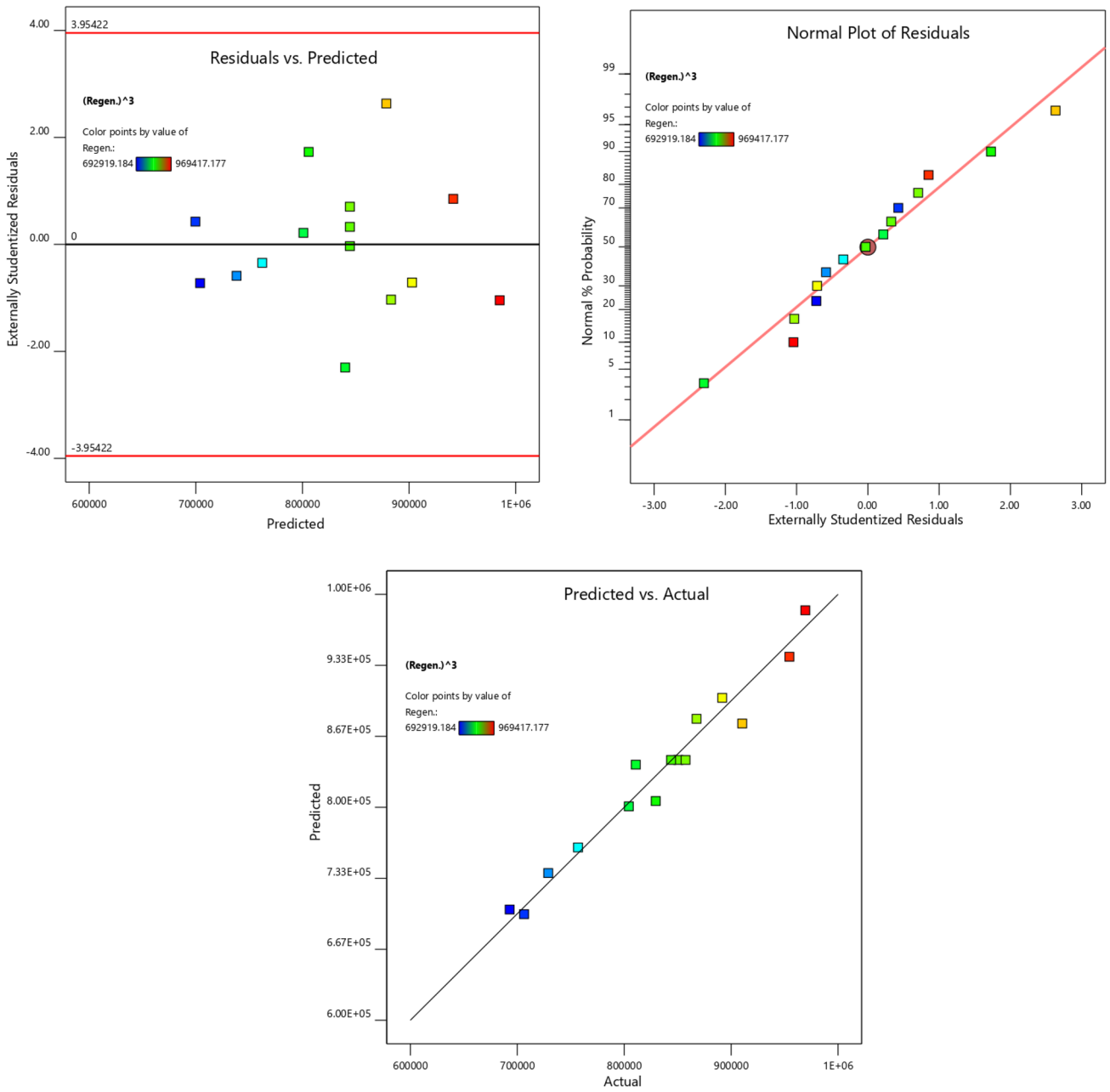

Fig. 10 Diagnosis plots of the regeneration model for zeolite 13X including the predicted vs. actual plot, residuals vs. predicted plot and normal plot of residuals

Table 8 Validation of the regeneration model and its experimental results for zeolite 13X contaminated with CO_2 under optimal conditions

No.	Initial concentration of CO_2 (A) ($ppm\ CO_2$)	Hot air temperature (B) (°C)	Contact time (C) (min.)	Capacity of fresh zeolite 13X ($mgCO_2\ g^{-1}$)	Capacity of regenerated zeolite 13X ($mgCO_2\ g^{-1}$)	Response (%)
1	1000	273	144	271.18	267.00	98.46 (99.44)*
2	2000	300	154	397.80	381.89	96.00 (96.75)
3	3000	300	154	530.40	494.07	93.15 (93.45)

*The predicted response is in the parenthesis

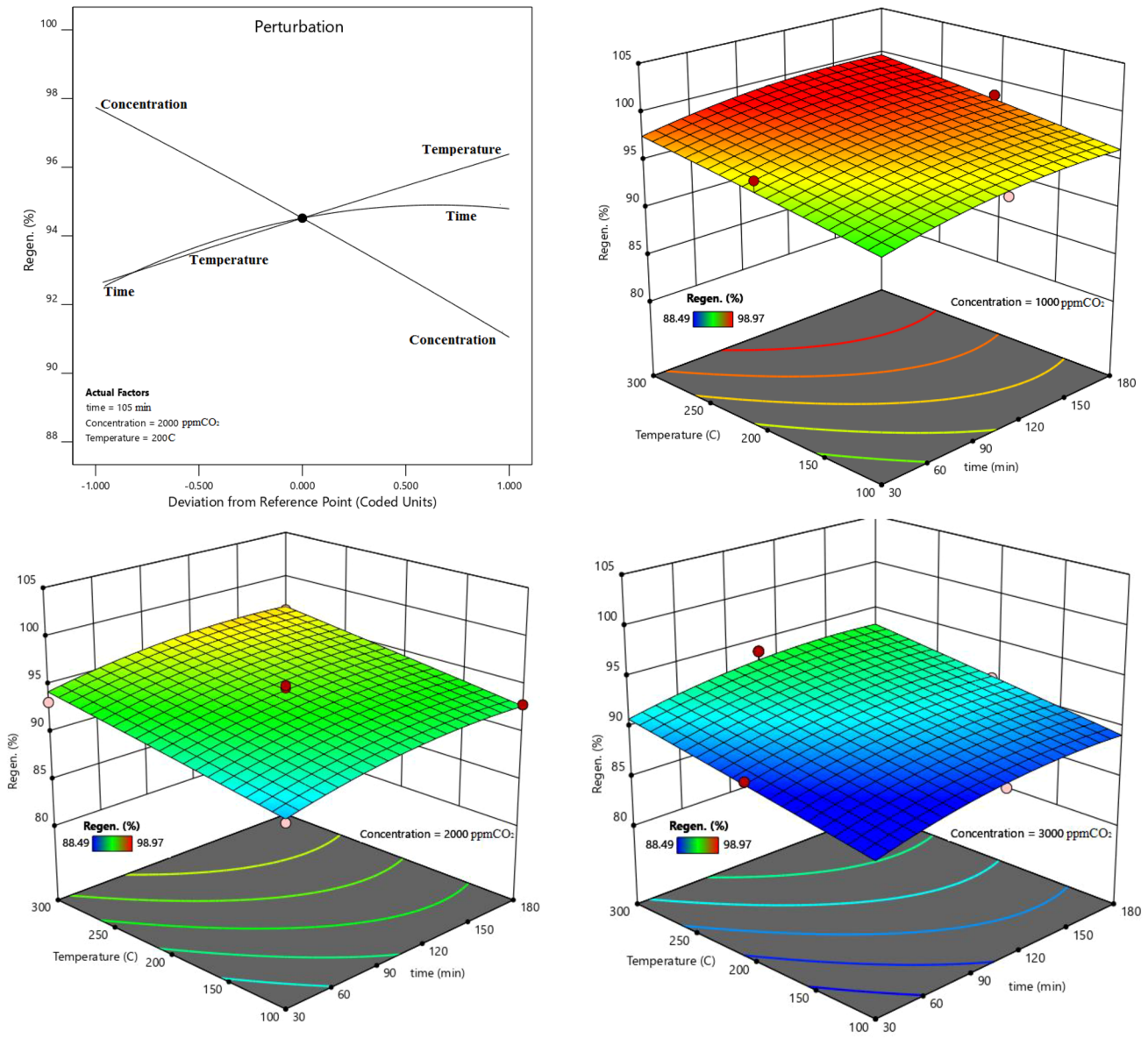

Fig. 11 Perturbation plot around the central point and combined effect of the hot air temperature and contact time on the zeolite 13X regeneration using the stagnant hot air contact method for various initial CO_2 concentrations

30 to 11 min for zeolite 13X powder by increasing the inlet CO_2 concentration from 1000 to 3000 ppm, while the mass transfer zone reduced until it remained constant for the inlet CO_2 concentration of more than 2000 ppm. As the pressure changed from 30 to 1 bar, the CO_2 breakthrough time decreased by 2.5-fold. Because, the pressure change affects the amount of adsorbate on the adsorbent surfaces demonstrating the mono-multilayer physical adsorption. Due to channeling, the CO_2 uptake decreased by around 50% for granular zeolite 13X compared to its powder in continuous mode.

The regeneration of zeolite 13X powder contaminated with CO_2 by the stagnant hot air contact method was evaluated using the Box–Behnken design in the atmospheric pressure. The experimental results indicated that the regeneration of zeolite 13X was highly sensitive to changing the initial CO_2 concentration so that its regeneration efficiency declined with the increased initial CO_2 concentration, which can be compensated by raising the air temperature or contact time.

Acknowledgements The authors are grateful to the Shiraz University for supporting this research.

Data Availability The data sets used and/or analyzed during the current study are available from the corresponding author on reasonable request.

Declarations

Conflict of interest The authors declare that they have no known competing financial interests or personal relationships that could have appeared to influence the work reported in this paper.

References

1. M.E. Olvera-Martínez, J. Mendoza-Flores, J. Genesca, CO2 corrosion control in steel pipelines. Influence of turbulent flow on the performance of corrosion inhibitors. J. Loss Prev. Process Ind. **35**, 19–28 (2015)
2. R. Dey, A. Samanta, Microwave-synthesized high-performance mesoporous SBA-15 silica materials for CO2 capture. Korean J. Chem. Eng. **37**, 1951–1962 (2020)
3. C.H. Lee, S.W. Park, S.S. Kim, Breakthrough analysis of carbon dioxide adsorption on zeolite synthesized from fly ash. Korean J. Chem. Eng. **31**, 179–187 (2014)
4. J. Xu, H. Wu, Z. Wang, Z. Qiao, S. Zhao, J. Wang, Recent advances on the membrane processes for CO2 separation. Chin. J. Chem. Eng. **26**(11), 2280–2291 (2018)
5. J.H. Choi, M.J. Park, J.N. Kim, Y. Ko, S.H. Lee, I. Baek, Modelling and analysis of pre-combustion CO2 capture with membranes. Korean J. Chem. Eng. **30**, 1187–1194 (2013)
6. H. Onyeaka, and O. C. Ekwebelem, A review of recent advances in engineering bacteria for enhanced CO_2 capture and utilization, Int. J. Environ. Sci. Technol. **20**, 4635–4648 (2023)
7. A. Goli, A. Shamiri, A. Talaiekhozani, N. Eshtiaghi, N. Aghamohammadi, M.K. Aroua, An overview of biological processes and their potential for CO2 capture. J. Environ. Manage. **183**, 41–58 (2016)
8. S. Campanari, P. Chiesa, G. Manzolini, CO2 capture from combined cycles integrated with Molten Carbonate Fuel Cells. Int. J. Greenhouse Gas Control **4**(3), 441–451 (2010)
9. F. Li, F. Mocci, X. Zhang, X. Ji, A. Laaksonen, Ionic liquids for CO2 electrochemical reduction. Chin. J. Chem. Eng. **31**, 75–93 (2021)
10. A. Wilk, L. Więcław-Solny, A. Tatarczuk, A. Krótki, T. Spietz, T. Chwoła, Solvent selection for CO2 capture from gases with high carbon dioxide concentration. Korean J. Chem. Eng. **34**, 2275–2283 (2017)
11. A.A. Khan, G. Halder, A.K. Saha, Kinetic effect and absorption performance of piperazine activator into aqueous solutions of 2-amino-2-methyl-1-propanol through post-combustion CO2 capture. Korean J. Chem. Eng. **36**, 1090–1101 (2019)
12. H. Dashti, L.Z. Yew, X. Lou, Recent advances in gas hydrate-based CO2 capture. J. Natl. Gas Sci. Eng. **23**, 195–207 (2015)
13. J.W. Lee, P. Dotel, J. Park, J.H. Yoon, Separation of CO2 from flue gases using hydroquinone clathrate compounds. Korean J. Chem. Eng. **32**, 2507–2511 (2015)
14. K.T. Chue, J.N. Kim, Y.J. Yoo, S.H. Cho, R.T. Yang, Comparison of activated carbon and zeolite 13X for CO2 recovery from flue gas by pressure swing adsorption. Ind. Eng. Chem. Res. **34**(2), 591–598 (1995)
15. J.S. Lee, J.H. Kim, J.T. Kim, J.K. Suh, J.M. Lee, C.H. Lee, Adsorption equilibria of CO2 on zeolite 13X and zeolite X/activated carbon composite. J. Chem. Eng. Data **47**(5), 1237–1242 (2002)
16. D.P. Bezerra, R.S. Oliveira, R.S. Vieira, C.L. Cavalcante, D.C.S. Azevedo, Adsorption of CO2 on nitrogen-enriched activated carbon and zeolite 13X. Adsorption **17**, 235–246 (2011)
17. R.V. Siriwardane, M.S. Shen, E.P. Fisher, J.A. Poston, Adsorption of CO2 on molecular sieves and activated carbon. Energy Fuels **15**(2), 279–284 (2001)
18. D. Bonenfant, M. Kharoune, P. Niquette, M. Mimeault, R. Hausler, Advances in principal factors influencing carbon dioxide adsorption on zeolites. Sci. Technol. Adv. Mater. **9**(1), 013007 (2008)
19. F. Gholipour, M. Mofarahi, Adsorption equilibrium of methane and carbon dioxide on zeolite 13X: Experimental and thermodynamic modeling. J. Supercrit. Fluids **111**, 47–54 (2016)
20. S. Kumar, The effect of elevated pressure, temperature and particles morphology on the carbon dioxide capture using zinc oxide. J. CO2 Util. **8**, 60–66 (2014)
21. D. Gouvêa, S.V. Ushakov, A. Navrotsky, Energetics of CO2 and H2O adsorption on zinc oxide. Langmuir **30**(30), 9091–9097 (2014)
22. Q.L. Tang, Q.H. Luo, Adsorption of CO2 at ZnO: a surface structure effect from DFT+ U calculations. J. Phys. Chem. C **117**(44), 22954–22966 (2013)
23. M.G. Olivier, R. Jadot, Adsorption of light hydrocarbons and carbon dioxide on silica gel. J. Chem. Eng. Data **42**(2), 230–233 (1997)
24. R. Roque-Malherbe, R. Polanco-Estrella, F. Marquez-Linares, Study of the interaction between silica surfaces and the carbon dioxide molecule. J. Phys. Chem. C **114**(41), 17773–17787 (2010)
25. Y. Zhao, Y. Shen, L. Bai, Effect of chemical modification on carbon dioxide adsorption property of mesoporous silica. J. Colloid Interface Sci. **379**(1), 94–100 (2012)
26. C. Lu, H. Bai, F. Su, W. Chen, J.F. Hwang, H.H. Lee, Adsorption of carbon dioxide from gas streams via mesoporous spherical-silica particles. J. Air Waste Manag. Assoc. **60**(4), 489–496 (2010)
27. F. de Correia Carvalho, P.F. do Nascimento, M.R. de Oliveira-Souza, A. Souza Araujo, 'The efficiency of bimodal silica as a carbon dioxide adsorbent for natural gas treatment. Processes **8**(3), 289 (2020)
28. S. Builes, S.I. Sandler, R. Xiong, Isosteric heats of gas and liquid adsorption. Langmuir **29**(33), 10416–10422 (2013)
29. M. R. Zaeri, and F. Esmaeilzadeh, Hydrogen sulfide removal from normal heptane using zinc oxide, silicon dioxide and zeolite 13X: adsorption capacity, kinetics, selectivity, breakthrough and regeneration, Environ. Sci. Pollut. Res. **30**, 84314–84333 (2023)
30. T.H. Hung, X. Deng, Q. Lyu, L.C. Lin, D.Y. Kang, Coulombic effect on permeation of CO2 in metal-organic framework membranes. J. Membr. Sci. **639**, 119742 (2021)